Retrieval of Microwave Surface Emissivities at TMI Frequencies in Shouxian

HONG Gang *[1,2] (洪 刚), Georg HEYGSTER[1], Klaus KUNZI[1], LI Wanbiao [2](李万彪), ZHU Yuanjing [2](朱元竞), and ZHAO Bolin [2](赵柏林)

[1] *Institute of Environmental Physics, University of Bremen, Post-box* 330440 28334, *Bremen, Germany*

[2] *Department of Atmospheric Sciences, School of Physics, Peking University, Beijing* 100871

(Received January 18, 2002; revised December 3, 2002)

ABSTRACT

Using a microwave radiative transfer model, atmospheric sounding profiles, satellite brightness temperatures, and some surface observed measurements under cloud-free conditions, surface emissivities at the frequencies of TRMM/TMI (Tropical Rainfall Measuring Mission Microwave Imager) at Shouxian in HUBEX (Huaihe River Basin Energy and Water Cycle Experiment) are retrieved. Compared to the microwave surface emissivities with changing conditions of the surface, it is found that the microwave emissivities have some sensitive variability with the conditions of the surface, and the variability is reasonable. In the calculation, the surface air temperatures are assumed to equal the surface skin temperatures, and only the emissivity at Shouxian is calculated; the calculation of the emissivities over the region of HUBEX needs more measurements.

Key words: microwave surface emissivities, TRMM/TMI

1. Introduction

Microwave radiometric land surface properties play an important role in many microwave remote sensing methods, including surface characterization, soil moisture estimation, and retrievals of atmospheric temperature, water vapor, cloud liquid water, and rainfall over land (Jones and Vonder Haar, 1997). In most of the atmospheric studies, simulations using microwave radiative transfer models are required. The emissivities of different surface types are large and highly variable, so accurate knowledge of microwave land surface emissivities will improve the precision of atmospheric microwave remote sensing.

Ground-based, aircraft, and satellite radiometers have been used to measure the emissivities of different surfaces at different frequencies and polarizations. Jones and Vonder Haar (1990) used the high sensitivity of the 85 GHz channels of Special Sensor Microwave Imager (SSM/I) to retrieve the cloud liquid water over the central United States. In order to minimize the effects of the surface emissivity variability, they estimated the surface emissivity under clear-sky conditions using coincident measurements from SSM/I, the surface skin temperature retrieved from the Visible (VIS) and Infrared (IR) Spin Scan Radiometer in geosynchronous orbit, and measurements of the atmospheric temperature and water vapor profiles from in situ sounding (Jones and Vonder Haar, 1997).

Recent work by Jones and Vonder Haar (1997) is an improvement over the previous method (Jones and Vonder Haar, 1990), including a surface skin temperature retrieval and a dynamic cloud discrimination method, in addition to an explicit atmospheric correction based on in situ atmospheric sounding. To calculate the atmospheric attenuation effects, microwave satellite data, infrared satellite data, and in situ atmospheric sounding data were used. Prigent et al. (1997, 1998, 1999) have done much work on estimating microwave land surface emissivities from SSM/I observations. Visible and infrared satellite observations were used to isolate the cloud-free SSM/I pixels. Then, the cloud-free atmospheric contribution was calculated from an estimate of the local atmospheric temperature and humidity profiles. The surface skin temperature was derived from IR observations. Finally, the surface emissivity was calculated by the integrated radiative transfer equation for a non-scattering plane-

*E-mail: honggang@uni-bremen.de

parallel atmosphere.

The method used here is based on the above methods, but the emissivity is not calculated in the same way. The microwave surface emissivities are simulated with VDISORT (Vector Discrete Ordinate Radiative Transfer) (Weng, 1992). Moreover, the microwave surface emissivity is set to 0 and 1 respectively, and then the simulated microwave brightness temperatures, the observed microwave brightness temperatures, and the land surface temperatures, are used to calculate the microwave surface emissivities.

2. VDISORT model and data

The model VDISORT is used to simulate the brightness temperature of the TRMM/TMI. First a method to discretize the integer-differential vector radiative transfer equation including both solar and thermal radiation is established. Then, a complete solution and boundary conditions in the context of the discrete ordinate method are constructed. VDISORT is able to compute the polarized radiative transfer under various atmospheric conditions. In this study, the land surface emissivity and atmospheric sounding profiles are used as input in order to simulate the brightness temperature at the top of the atmosphere under cloud-free conditions.

The TRMM satellite was jointly developed by NASDA and NASA and launched from NASDA's Tanegashima Space Center on November 1997 into a near circular, non-sun-synchronous orbit of approximately 350 km altitude with an inclination of 35 degrees and a period of 91.5 minutes (15.7 orbits per day). TRMM is an earth observation satellite making global measurements of the tropical and sub-tropical rainfall. The instruments include microwave and visible infrared sensors, and the first spaceborne rain radar. Its orbit ranges between 35° north and 35° south of the equator. TMI aboard TRMM is provided by NASA, and operates in a conical scan mode, with a constant ground surface incidence angle of 52.76° The scan angle of the TMI antenna is 130° producing a swath width of 758.5 km. The detailed TMI characteristics are shown in Table 1 (Kummerow et al., 1998).

Table 1. TRMM/TMI Instrument Characteristics

Channel Number	1,2	3,4	5	6,7	8,9
Center Frequency (GHz)	10.65	19.35	21.3	37.0	85.5
Polarization	V, H	V, H	V	V, H	V, H
Effective Field of View (km × km)	63×37	30×18	23×18	16×9	7×5

In this study the TMI data in conjunction with HUBEX observations from June to July 1998 are used. First, we chose an area of latitude between 32.5°N and 32.6°N, and longitude between 116.7°E and 116.8°E. The atmospheric conditions taken from Fuyang station (32.93°N, 115.83°E) are assumed to be horizontally constant within the TMI pixels covering the HUBEX region, while the synoptic observations from Shouxian station (32.55°N, 116.78°E) are used. Then we assigned the average value of brightness temperatures in this area as the brightness temperature at Shouxian station.

Observational measurements from six stations include cloud information, high-resolution upper air sounding data observed at Fuyang station in HUBEX. Because our study was focused on Shouxian, we only used the high-resolution upper air sounding data observed at Fuyang. The time resolution is 10 seconds at Fuyang, and the observation took about one hour. During 1–10 June and 23–31 July 1998, there were only two observations (0000, 1200 UTC) per day for measurements of the high-resolution atmospheric sounding profiles. From 11 June to 22 July, there were four observations (0000, 0600, 1200, 2000 UTC) per day of this type. The sounding profiles contain the pressure, altitude, temperature, dew-point temperature, relative humidity, wind direction, and wind velocity. We used the Goff-Gratch formula to convert the dew-point temperature measurements to mixing ratios, which is one input of the VDISORT model. For the simulation, we chose the sounding profiles observed within about one hour of the TMI pass over Shouxian.

In this study, only cloud-free cases are considered, and this was checked from observational data. There are 24 surface observations at Shouxian station in HUBEX, including the surface air temperature and cloud information, etc. At the same time, we used the surface air temperatures as estimates of surface skin temperatures needed as input for the VDISORT model.

3. Method to determine the microwave surface emissivities

Felde and Pickle (1995) calculated the surface emis-

sivity ε_s at 91 GHz and 150 GHz under cloud-free conditions as

$$\varepsilon_s = (TB - c_1c_2 - c_3)/(c_2T_s - c_1c_2), \quad (1)$$

with TB the brightness temperature observed by the satellite sensor, T_s the surface skin temperature, and c_1, c_2, and c_3 denoting the downwelling atmospheric emission, net atmospheric transmissivity, and upwelling atmospheric emission respectively. Parameters, c_1, c_2, and c_3 were calculated with the Eyre SSM/T2 simulation model, which was given the atmospheric profile, path zenith angle, and microwave frequency. In this study, we set ε_s=0 and ε_s=1 respectively. With the atmospheric sounding profiles and the observed surface air temperature, we can determine (Liou, 1980),

$$\begin{aligned} L_v(0) = {} & \varepsilon_v B_v(T_s)\tau_v(p_s,0) + \\ & \int_{p_s}^{0} B_v[T(p)]\frac{\partial \tau_v(p,0)}{\partial p}dp \\ & +(1-\varepsilon_v)[\tau_v(p_s,0)]^2 \\ & \int_{p_s}^{0} \frac{B_v[T(p)]}{[\tau_v(p,0)]^2}\frac{\partial \tau_v(p,0)}{\partial p}dp \\ & +(1-\varepsilon_v)[\tau_v(p_s,0)]^2 B_v(T_{\text{space}}), \end{aligned} \quad (2)$$

where $L_v(0)$ is the upward radiance observed by the satellite at pressure $p = 0, v$, is the frequency, ε_v is the surface emissivity at the frequency $v, B(T)$ is the Planck function for a temperature $T, \tau(p_s, 0)$ is the atmospheric transmittance for the whole atmospheric layer, T_s is the surface skin temperature, p_s is the surface pressure, and T_{space} is the cosmic emission temperature (about 2.7 K). The four terms on the right-hand side of (2) are the surface term, the direct upward atmospheric emission, the downward atmospheric emission reflected from the surface, and the cosmic radiation reflected from the surface, respectively. Based on (2), we can calculate the surface emissivity ε_v,

$$\begin{aligned} \varepsilon_v = {} & \Big\{L_v(0) - \int_{p_s}^{0} B_v[T(p)]\frac{\partial \tau_v(p,0)}{\partial p}dp \\ & - [\tau_v(p_s,0)]^2 \int_{p_s}^{0} \frac{B_v(T(p))}{[\tau_v(p,0)]^2}\frac{\partial \tau_v(p,0)}{\partial p}dp \\ & - [\tau_v(p_s,0)]^2 B_v(T_{\text{space}})\Big\} / \Big\{B_v(T_s)\tau_v(p_s,0) \\ & - [\tau_v(p_s,0)]^2 B_v(T_{\text{space}}) \\ & - [\tau_v(p_s,0)]^2 \int_{p_s}^{0} B_v[T(p)]\frac{\partial \tau_v(p,0)}{\partial p}dp\Big\}. \end{aligned} \quad (3)$$

Based on (2), if the surface emissivity ε_v is set to 0, we get

$$\begin{aligned} L'_v(0) = {} & \int_{p_s}^{0} B_v[(T(p)]\frac{\partial \tau_v(p,0)}{\partial p}dp \\ & + [\tau_v(p_s,0)]^2 \int_{p_s}^{0} \frac{B_v[T(p)]}{\tau_v(p,0)]^2}\frac{\partial \tau_v(p,0)}{\partial p}dp \\ & + [\tau_v(p_s,0)]^2 B_v(T_{\text{space}}). \end{aligned} \quad (4)$$

If the surface emissivity ε_v is set to 1, we get

$$\begin{aligned} L''_v(0) = {} & B_v(T_s)\tau_v(p_s,0) \\ & + \int_{p_s}^{0} B_v[T(p)]\frac{\partial \tau_v(p,0)}{\partial p}dp, \end{aligned} \quad (5)$$

and then (3) is easily denoted as

$$\varepsilon_v = [L_v(0) - L'_v(0)]/[L''_v(0) - L'_v(0)]. \quad (6)$$

In the microwave region, the Rayleigh-Jeans approximation $B_v = \dfrac{2v^2kT}{c^2}$, is used for TMI, where v is the microwave frequency, B is the blackbody brightness, k is the Boltzmann constant, c is the speed of light, and T is the absolute temperature. With the Rayleigh-Jeans formula, we can calculate ε_v by

$$\varepsilon_v = [T_v(0) - T'_v(0)]/[T''_v(0) - T'_v(0)], \quad (7)$$

where $T_v(0)$ is the brightness temperature observed by TMI, $T'_v(0)$ is the simulated brightness temperature with $\varepsilon_v = 0$ by the VDISORT model, $T''_v(0)$ is the simulated brightness temperature with ε_v=1 by the VDISORT model. Then with (7), we can get the microwave surface emissivities. Quantities $T'_v(0)$ and $T''_v(0)$ can be determined from the known atmospheric profile only: the microwave surface emissivity is not needed.

4. Simulation

In order to check the accuracy of the method, we chose in situ data of 0800 LST 11 July for the simulation. The surface emissivity was varied from 0.5 to 1.0, and then we calculated the brightness temperatures with VDISORT. The retrieved microwave emissivities were calculated by the simulated brightness temperatures together with the simulated brightness temperatures when $\varepsilon_v = 0$ and $\varepsilon_v = 1$. Then the assumed emissivities and retrieved emissivities were compared as shown in Fig. 1, and the retrieved emissivities were compared to the assumed emissivities in Fig. 2. Here we only present results for the frequencies 10 GHz and 85 GHz, the results for the other frequencies being similar. As we see from Fig. 1, the theoretical accuracy of the retrieval method is very high. The difference between the retrieved surface emissivity and the assumed surface emissivity is below 0.0005 (10, 19 and 37 GHz), 0.0013 (85 GHz) for all considered cases (0.5

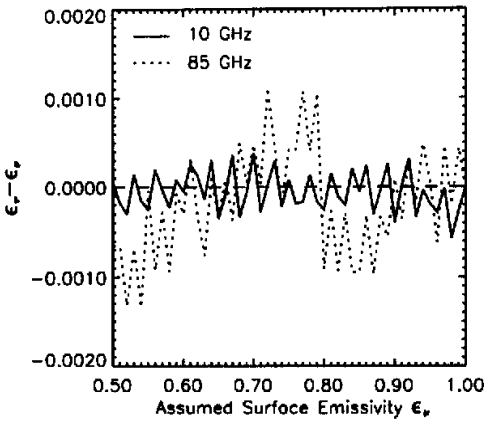

Fig. 1. The difference between the retrieved surface emissivity and the assumed surface emissivity versus the assumed emissivity.

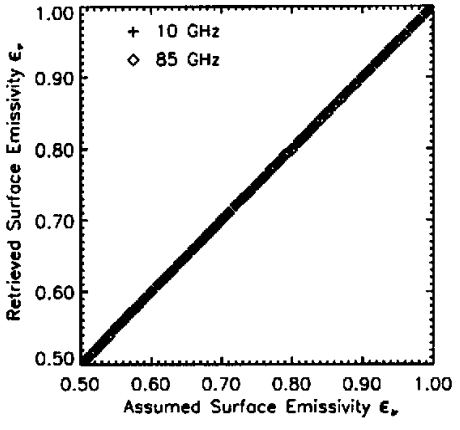

Fig. 2. The retrieved surface emissivity versus the assumed surface emissivity.

$< \varepsilon_v <1.0$), hence this method is able to determine the surface emissivity.

5. Surface emissivities results and discussion

According to this retrieval method, the retrieved surface emissivities are shown in Table 2. Unfortunately, there are no actual observed surface emissivities to check the results of procedure. In order to check the accuracy of the method, we calculated the surface emissivity polarization differences at 10, 19, 37, and 85 GHz. Figure 3 shows that the surface emissivity polarization differences (a, b), the vertical polarization emissivity (c), and the precipitation (d) change with time. We find that the variances of the polarization differences at 10, 19, and 37 GHz have similar trends, and their variances are small. In contrast, the polarization differences at 85 GHz show a high variance. The lower frequencies (10, 19 GHz) of TMI have large transmissivity; they can reflect information about the surface. Microwave observations have been shown to be valuable for delineating a flooded area (Choudhury, 1989), and the surface emissivity polarization difference has been found to be a good visual indicator of the surface wetness (Jones and Vonder Haar, 1997). Because of the differences in the dielectric properties of water as compared with soil and vegetation and the flatness of standing water surfaces, at microwave frequencies, open water and flooding decrease the emissivities in both polarizations and increase the polarization differences, especially at lower frequencies (Prigent et al., 1998). Because there are no direct measurements of surface emissivities at Shouxian, it is difficult to verify the retrieved surface emissivities. In this paper, instead, comparisons of the variations of the surface emissivities and surface characteristics are used to verify the retrieved surface emissivities.

11–17 June (Day 11–17) This period was in the earlier stage of the breaking of Meiyu, From 2100 LST 11 June to 2000 LST 12 June, the precipitation was about 16.7 mm, and the precipitation of the following 8 hours was near 0.0 mm. The retrieved surface emissivities (10 and 19 GHz) on 13, and 14, June were low and ranged from about 0.79 to 0.82; the emissivities on 16 June were about 0.83. At the same time, the polarization differences of 10, 19, and 37 GHz were large and about 0.15. This response was due to the wetland caused by the precipitation. From 13 to 17 June, there was no precipitation. The wetland became dry, and then the emissivities (10 and 19 Ghz) increased to about 0.83 and 0.84. However, the emissivity polarization differences of 10 and 19 GHz decreased to about 0.13 and 0.10.

18–28 June (Day 18–28) This period was still in the earlier stage of the breaking of Meiyu. There were only two precipitation events of about 0.2 mm in this period, one on 18 June and the other on 25 June. The retrieved surface emissivities (10 and 19 GHz) on 22 June were about 0.84. The retrieved surface emissivities (10 and 19 GHz) on 28 June ranged from about 0.86 to 0.90. The trend of the emissivities in this period is increasing. At the same time, the trend of the surface emissivity polarization difference is decreasing.

29 June–5 July (Day 29–35) This period was still one part of Meiyu, especially the period from 29 June to 3 July, which was the main period of Meiyu. The precipitation in this period was about 300 mm, and the land was wet. So the surface emissivities should be lower and the surface emissivity polarization differences should be larger, which is confirmed in Fig. 3. The retrieved surface emissivities (10 and 19 GHz) on 5 July were about 0.81, and the emissivity polarization differences of 10 and 19 GHz were increased to about 0.13.

6–12 July (Day 36–42) There was no precipitation in this period; the wetland dried successively more and more.

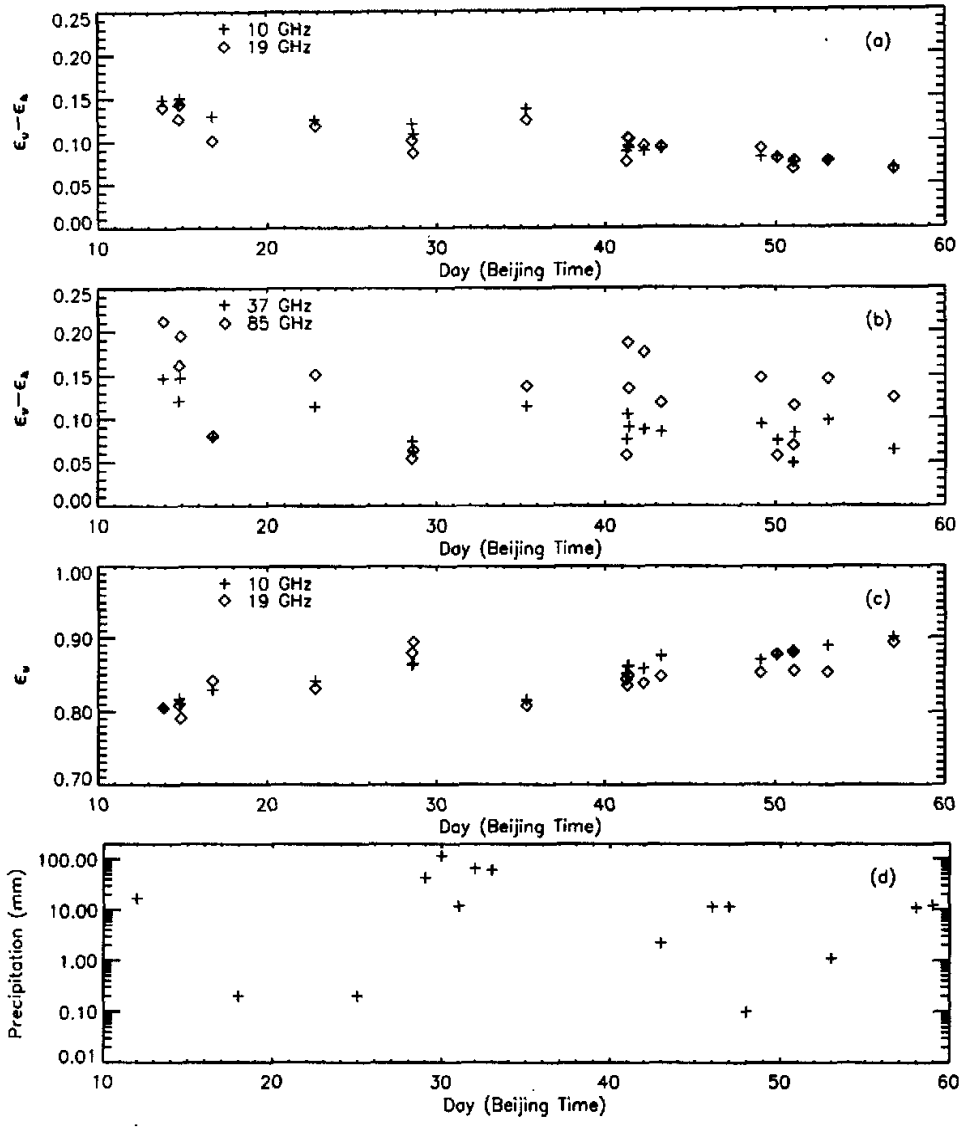

Fig. 3. The microwave surface emissivity polarization differences at 10 and 19 GHz (a), at 37 and 85 GHZ (b), the vertical polarization emissivity at 10 and 19 GHz (c), the precipitation at Shouxian (d) versus the local time.

Table 2. The Results of the Microwave Surface Emissivities at Shouxian in HUBEX

Case	Time	10v	10h	Δ10	19v	19h	Δ19	21v	37v	37h	Δ37	85v	85h	Δ85
1	6132055	0.8051	0.6566	0.1485	0.8058	0.6656	0.1429	0.8080	0.8118	0.6645	0.1473	0.8414	0.6292	0.2122
2	6141942	0.8168	0.6737	0.1431	0.8095	0.6832	0.1263	0.8127	0.8275	0.7070	0.1205	0.8737	0.7117	0.1620
3	6142120	0.8110	0.6615	0.1495	0.7913	0.6480	0.1433	0.7967	0.8091	0.6617	0.1474	0.8168	0.6217	0.1951
4	6161854	0.8290	0.6991	0.1299	0.8416	0.7400	0.1016	0.8533	0.8696	0.7904	0.0792	0.8827	0.8023	0.0804
5	6221942	0.8409	0.7159	0.1250	0.8309	0.7125	0.1184	0.8341	0.8417	0.7277	0.1140	0.8497	0.6982	0.1515
6	6281227	0.8629	0.7424	0.1205	0.8793	0.7778	0.1015	0.8911	0.9076	0.8332	0.0744	0.9686	0.9140	0.0546
7	6281405	0.8651	0.7566	0.1085	0.8947	0.8079	0.0868	0.9061	0.9129	0.8510	0.0619	0.9580	0.8940	0.0640
8	7050849	0.8156	0.6781	0.1375	0.8082	0.6833	0.1249	0.8153	0.8259	0.7116	0.1143	0.8235	0.6854	0.1381
9	7110623	0.8516	0.7637	0.0879	0.8438	0.7673	0.0765	0.8433	0.8716	0.7952	0.0764	0.8478	0.7894	0.0584
10	7110800	0.8611	0.7666	0.0945	0.8354	0.7315	0.1039	0.8245	0.8481	0.7429	0.1052	0.8512	0.6638	0.1874
11	7110937	0.8620	0.7697	0.0923	0.8490	0.7460	0.1030	0.8409	0.8614	0.7708	0.0906	0.8696	0.7341	0.1355
12	7120647	0.8588	0.7707	0.0881	0.8384	0.7438	0.0946	0.8316	0.8663	0.7786	0.0877	0.8830	0.7067	0.1763
13	7130712	0.8752	0.7840	0.0912	0.8476	0.7546	0.0930	0.8537	0.8661	0.7812	0.0849	0.8776	0.7589	0.1187
14	7190309	0.8698	0.7890	0.0808	0.8527	0.7614	0.0913	0.8473	0.8461	0.7525	0.0936	0.8071	0.6596	0.1475
15	7200156	0.8758	0.7946	0.0812	0.8774	0.7979	0.0795	0.8664	0.8762	0.8014	0.0748	0.8557	0.7984	0.0573
16	7210044	0.8822	0.8081	0.0741	0.8802	0.8127	0.0675	0.8770	0.8897	0.8407	0.0490	0.8648	0.7955	0.0693
17	7210221	0.8810	0.8066	0.0744	0.8552	0.7784	0.0768	0.8509	0.8649	0.7812	0.0837	0.8152	0.6998	0.1154
18	7230133	0.8895	0.8139	0.0756	0.8534	0.7771	0.0763	0.8559	0.8601	0.7619	0.0982	0.8742	0.7277	0.1465
19	7262219	0.9008	0.8316	0.0692	0.8938	0.8273	0.0665	0.9034	0.9011	0.8369	0.0642	0.9325	0.8079	0.1246

The format of the time is MDDHHMM (Beijing Time), and Δ means the difference between the vertical polarized emissivity and the horizontally polarized emissivity, v and h mean vertical and horizontal polarization respectively.

The retrieved surface emissivities (10 and 19 GHz) increased and the emissivity polarization differences (10, 19 and 37 GHz) decreased to less than 0.10.

13–27 July (Day 43–57) The main precipitation events in this period occurred on 16 and 17 July, and the total precipitation was about 33 mm. On 23 July the precipitation was about 1.1 mm, so from 18 to 27 July, the period can be regarded as a dry period, and the land surface became more and more dry. Comparing Figs. 3 a and c, the correspondence between the surface emissivities and the variations in surface characteristics is obvious. The moisture of the land soil decreased, then the surface emissivities increased and the emissivity polarization difference decreased.

Based on the above analysis, the correspondence between the surface emissivities and the variations in the surface characteristics verifies that the calculated emissivities are reasonable and the method of calculating the emissivity is also reasonable.

6. Conclusion

Combining the atmospheric sounding profiles, the brightness temperatures at the top of the atmosphere observed by TMI, and some surface-observed measurements under cloud-free conditions, microwave surface emissivities are estimated from TMI observations. The microwave surface emissivities are calculated at Shouxian for June and July 1998. In this method, we use the surface air temperatures as the surface skin temperatures. This hypothesis will lead to some errors in the retrieval. Jones and Vonder Haar (1997) and Prigent et al. (1997, 1998, 1999) calculated the surface skin temperature with the help of the visible and infrared satellite observations. The surface observations of the surface temperature are usually taken only fours times per day, thus it is difficult to get the in situ surface temperatures at the times of the satellite observations. So estimating the surface skin temperature from the infrared satellite data can improve the precision of the calculated surface emissivity. Some methods to determine the land surface temperature from infrared satellite data have been discussed in the past (Sobrino et al., 1991; Kerr et al., 1992; Crago et al., 1995; Wan and Dozier, 1996; Pozo Vazquez et al., 1997). In our future research, a surface skin temperature retrieval algorithm will be first used to obtain accurate land skin temperatures. Then, we can obtain the land microwave surface emissivities. In particular, using infrared satellite data, the spatial land surface

temperature can be calculated. Based on the calculated distribution of the surface skin temperature, the surface emissivities in the region can be calculated using the method given here.

This paper calculates the emissivities in Shouxian for two months, with changes of the weather situation and the precipitation during the period, and compares the relation between the surface emissivities and the surface wetness. The variations of the surface emissivities and the emissivity polarization difference are found to obey the same rule as pointed out by Jones and Vonder Haar (1997) and Prigent et al. (1997, 1998). As they said, the microwave surface emissivity polarization difference can be a good qualitative indicator of the surface wetness.

Acknowledgments. This work was supported by the National Natural Science Foundation of China under Grant Nos. 49794030 and 40105001. The authors wish to thank the reviewers for their careful reading of this paper and their helpful suggestions. The authors also thank Li Zhenglong for his useful comments. Gang Hong is grateful to the Gottlieb Daimler-und Karl Benz-Stiftung and the office team of the foundation for the support of the fellowship program.

REFERENCES

Choudhury, B. J., 1989: Monitoring global land surface using Nimbus-7 37 GHz data: Theory and examples. *Int. J. Remote Sens.*, **10**, 1579–1605.

Crago, R., M. Sugita, and W. Brutsaert, 1995: Satellite-derived surface temperatures with boundary layer temperatures and geostrophic winds to estimate surface energy fluxes. *J. Geophys. Res.*, **100**, 25447–25451.

Felde, G. W., and J. D. Pickle, 1995: Retrieval of 91 and 150 GHz Earth surface emissivities. *J. Geophys. Res.*, **100**, 20855–20866.

Jones, A. S., and T. H. Vonder Haar, 1990: Passive microwave remote sensing of cloud liquid water over land regions. *J. Geophys. Res.*, **95**, 16673–16683.

Jones, A. S., and T. H. Vonder Haar, 1997: Retrieval of microwave surface emittance over land using coincident microwave and infrared satellite measurements. *J. Geophys. Res.*, **102**, 13609–13626.

Kerr, Y. H., J. P. Lagourde, and J. Imbernon, 1992: Accurate land-surface temperature retrieval from AVHRR data with the use of an improved split-window algorithm. *Remote Sens. Environ.*, **41**, 197–209.

Kummerow, C., W. Barnes, T. Kozu, J. Shiue, and J. Simpson, 1998: The tropical rainfall measuring mission (TRMM) sensor package. *J. Atmos. Oceanic Technol.*, **15**, 809–817.

Liou, K., 1980: *An Introduction to Atmospheric Radiation*, Academic Press. New York, 392 pp.

Pozo Vazquez, D., F. J. Olmo, and L. Alados-Arboledas, 1997: A comparative study of algorithms for estimating land surface temperature from AVHRR data. *Remote Sens. Environ.*, **62**, 215–222.

Prigent, C., W. B. Rossow, and E. Matthews, 1997: Microwave land surface emissivities estimated from SSM/I observations. *J. Geophys. Res.*, **102**, 21867–21890.

Prigent, C., W. B. Rossow, and E. Matthews, 1998: Global maps of microwave land surface emissivities: potential for land surface characterization. *Radio Sci.*, **33**, 745–751.

Prigent, C., W. B., Rossow, E. Matthews, and B. Marticorena, 1999: Microwave radiometric signatures of different surface types in deserts. *J. Geophys. Res.*, **104**, 12147–12158.

Sobrino, J. A., C. Coll, and V. Caselles, 1991: Atmospheric corrections for land surface temperature using AVHRR channel 4 and 5. *Remote Sens. Environ.*, **38**, 19–34.

Wan, Z., and J. Dozier, 1996: A generalized split-window algorithm for retrieving land-surface temperature from space. *IEEE Trans. Geosci. Remote Sens.*, **34**, 892–905.

Weng, F. Z., 1992: A multi-layer discrete-ordinate method for vector radiative transfer in a vertically-inhomogeneous, emitting and scattering atmosphere I: Theory. *J. Quant. Radiat. Transfer*, **47**, 19–35.

反演寿县TMI微波频率的地表比辐射率

洪 刚 Georg HEYGSTER Klaus KUNZI 李万彪 朱元竞 赵柏林

摘 要

利用一个微波辐射传输模式，晴天下的大气探测廓线，地面的部分观测资料以及卫星观测的亮温，计算了淮河流域能量和水循环实验(HUBEX)中，寿县地区的热带降雨观测卫星微波成像仪(TRMM/TMI) 微波频率的地表比辐射率。通过比较所计算的微波地表比辐射率随地表状况的改变，发现地表微波比辐射率随地表状况的变化存在敏感性，并且其变化是合理的。本文中，地表肤温设定等于地表空气温度，并且仅计算了寿县的地表比辐射率，在HUBEX区域上的地表比辐射率的计算需要更多的观测资料。

关键词: 微波地表比辐射率，热带降雨观测卫星微波成像仪